Experimental and theoretical investigation of the performance of an air to water multi-pass heat pipe-based heat exchanger

Hussam Jouhara [a],[*], Sulaiman Almahmoud [b], Daniel Brough [a], Valentin Guichet [a], Bertrand Delpech [a], Amisha Chauhan [a], Lujean Ahmad [a], Nicolas Serey [a]

[a] Heat Pipe and Thermal Management Research Group, College of Engineering, Design and Physical Sciences, Brunel University London, UB8 3PH, UK
[b] Spirax Sarco Engineering PLC, Cheltenham, GL51 9NQ, United Kingdom

ARTICLE INFO

ABSTRACT

In this paper, the performance of a multi-pass heat pipe-based heat exchanger (HPHE) is investigated experimentally and theoretically. The heat pipe system consists of copper heat pipes in a specific equatorially staggered configuration to facilitate heat transportation from a hot gas (air) to a water flow, which cools the condenser section of these heat pipes. The effect of the Reynolds number on the heat transfer rate was studied by altering the number of passes for the evaporator section for the same system by the incorporation of various baffles and by varying the water flow rate. The experimental results have highlighted the strong correlation between heat exchanger performance and the Reynolds number. By increasing the number of passes from one to five, the effectiveness of the HPHE was improved by more than 25%. It has been demonstrated that increasing the number of passes increases the Reynolds number of the flow, leading to higher heat transfer coefficients and lower thermal forced convection resistances. The HPHE overall performance, as well as, the outlet temperatures of the fluids were predicted through two theoretical models, based on the Log Mean Temperature Difference (LMTD) method and the Effectiveness-Number of Transfer Units (ε-NTU) method. The predictions were compared with experimental results and the accuracy of the models reported. The validation showed that the developed iterative LMTD model predicted the performance of the HPHE within $\pm 15.5\%$ error. In comparison, the ε-NTU model predicted the total effectiveness with a maximum error of 19% and was able to predict the outlet temperatures of both air and water streams within an accuracy of $\pm 0.7\ ^\circ$C. The reported research is of importance for the application of heat pipe heat exchangers in waste heat recovery. Finally, knowledge is provided on the accuracy of the available prediction models.

1. Introduction

A major challenge faced by Energy Intensive Industries (EIIs) is the large amount of thermal energy rejected during high temperature processes. For companies, the release of high temperature exhausts represents a tangible loss of money and is an obstacle to competitiveness. In accordance with modern economic concerns such as fluctuating oil prices, the high fossil fuel dependency of some countries, and, in addition, the rising awareness in industry of global warming, innovative heat recovery systems are being developed to reduce manufacturing costs with environmentally friendly solutions. For EIIs, the utilisation of heat exchangers, placed

within an exhaust stream, to recover waste heat is a promising solution [1]. However, the risk of stream cross-contamination or fouling in traditional technologies due to the exhaust gas composition is high. For these reasons, the installation of heat pipe-based heat exchangers (HPHEs) is becoming more prevalent throughout the industrial sector as they provide a high heat recovery performance whilst separating the hot and cold streams, thus eliminating the risk of contaminating the heat sink.

Recently, HPHEs have been tested in many domains such as heating, ventilation and air conditioning installations [2], heat recovery for hospitals [3], ceramics kilns [4–7], the steel industry [5,8,9], burners, boilers and preheaters [10], photovoltaic-thermal systems [11], data centre cooling [12], metal forging, automotive and nuclear applications [13], thermal storage [14], municipal waste treatment [15] among others. The success of HPHEs is also explained by key advantages related to heat pipes. Indeed, for the

Nomenclature

A	Surface area m^2
C	Heat capacity rate W.K^{-1}
C_P	Specific heat J.kg^{-1}.K^{-1}
C_r	Heat capacity ratio, ($C_r = C_{min}/C_{max}$) dimensionless
C_{sf}	Constant in *Rohsenow* correlation depending on the surface-fluid combination dimensionless
D	Diameter of heat pipe m
g	Gravitational acceleration m.s^{-2}
h	Heat transfer coefficient W.m^{-2}.K^{-1}
h_{fg}	Latent heat of vaporization J.kg^{-1}
k	Thermal conductivity W.m^{-1}.K^{-1}
L	Length m
$\dot{m}$	Mass flow rate kg.h^{-1} or l.s^{-1}
n	Number of rows dimensionless
Nu	Nusselt number, ($Nu = hD/k$) dimensionless
Pr	Prandtl number, ($Pr = \mu c_p /k$) dimensionless
Q	Heat transfer rate W
R	Thermal resistance °C.W^{-1}
Re	Reynolds number, ($Re = \rho VD/\mu$) dimensionless
S_L	Longitudinal pitch of the staggered arrangement m
S_T	Transverse pitch of the staggered arrangement m
T	Temperature °C
U	Overall heat transfer coefficient W.m^{-2}.K^{-1}
V	Velocity m.s^{-1}

Greek Symbols

Δ	Difference
ε	Effectiveness dimensionless
ρ	Density kg.m^{-3}
σ	Surface tension N.m^{-1}
μ	Dynamic viscosity Pa.s

Subscripts

1 *row*	For one row
air	Air
c	Condenser
cond	Conduction
e	Evaporator
hp	Heat pipe
l	Liquid
L	Longitudinal
LM	Logarithmic mean
max	Maximum
in	Inlet
int	Internal
o	Out
out	Outlet
s	Wall surface
sat	Saturation
t	Total
T	Transverse
ν	Vapour
w	Evaluated at wall
water	Water

Acronyms

CFD	Computational Fluid Dynamics
EII	Energy Intensive Industry
HPHE	Heat Pipe Heat Exchanger
LMTD	Log Mean Temperature Difference
PID	Proportional-Integral-Derivative
P&ID	Piping and Instrumentation Diagram
TPCT	Two-phase closed Thermosyphon
ε-NTU	Effectiveness-Number of Transfer Units

same heat transfer rate, the heat pipe technology permits a reduction in the size of the heat exchanger by optimising the pipe size and length, with minimal need for maintenance and an increased lifespan of more than twenty years [16]. For instance, the failure of a few heat pipes will have little impact on the overall thermal performance of the heat exchanger. The applicability range of such installations is also promoted by the small difference of temperature required between the hot and cold streams for efficient heat transfer. *Jouhara* [17] evaluated the energy and cost savings by integrating a wraparound heat pipe into conventional dehumidification and ventilation units. The wraparound heat pipe technology showed a payback period of less than a year for medium sized central unit. Moreover, heat pipes are considered as superconductors due to utilising two-phase heat transfer between the heat source and heat sink. *Jouhara* and *Robinson* [18] investigated experimentally a thermosyphon using Dowtherm A and Thermonol VP1 at working temperature up to 420 °C. The studied heat pipe showed an effective thermal conductivity up to 20 kW m^{-1} K^{-1}.

The performance of HPHEs depends on several factors such as the type and geometry of the heat exchanger, the flow direction, the heat exchange area, the mass flow rates and the temperature of both hot and cold streams [19,20]. Moreover, the fluid regime, which is described by the Reynolds number, plays a significant role in the heat transfer. It is commonly known that more turbulent flow increases the forced convection heat transfer coefficient. However, for a given increase in the Reynolds number, information regarding

the corresponding increase of the heat exchanger performance under different flow conditions has limited availability in literature. To adjust the Reynolds number of a stream for a constant flow rate, a mechanical solution is the introduction of baffles to change the number of passes in the heat exchanger. By decreasing the flow area, the Reynolds number and turbulence increase. Several studies have demonstrated the impact of changing the number of passes on the performance of a given system. *Ramos* et al. [21] and *Mroue* et al. [22] investigated both numerically and experimentally the performance of a similar air to water HPHE with one pass and two passes, respectively. The two experiments were conducted under the same conditions such as equivalent air and water inlet temperatures and mass flow rates, with the only variable being the number of passes. The experimental results confirmed an increase in the heat transfer rate with increasing mass flow rate and inlet temperature of the air stream. Yet, for constant conditions, authors observed that the effectiveness of the HPHE was degraded when increasing the air flow rate. In comparison between one pass and two passes, the heat transfer rate and total effectiveness of the heat exchanger was higher for two passes. *Kim* et al. [23] numerically optimized the number of passes of a heat exchanger using computational fluid dynamics. As an indicator, authors used the JF factor, a combination of the Colburn (j) and friction (f) factors and balanced the heat transfer improvement with the induced pressure drop to propose an optimum number of passes for their exchanger. Yet, the numerical results have not been validated experimentally.

Rao and Das [24] investigated a multi-pass plate heat exchanger and observed that, at a low number of passes, an increase in the fluid velocity can be counterproductive in terms of heat transfer enhancement. They also concluded that an increase in the heat transfer surface area can become ineffective if it implies a bad distribution of the flow. In this case, it seems that the flow distribution has had a higher impact on the heat transfer rate than the heat transfer area. However, the authors did not investigate the effect of the number of passes on the overall performance of the heat exchanger. Besides the advantage of HPHEs, a significant amount of detailed scientific research in this area is lacking. In particular, the impact of the number of passes and thus on the Reynolds number on the performance of a HPHE has been hardly reported, experimentally. This paper aims at bringing some knowledge to this gap in available publications.

For companies and engineers, the prediction of the performance of a system is also of interest and is required to estimate the return-on-investment period for a given installation. For potential investors at companies and EIIs, an accurate return on investment prediction is vital to increase confidence in the potential investment in a heat exchanger. To calculate the performance of a heat exchanger, two techniques are commonly used: the Log Mean Temperature Difference (LMTD) method and the effectiveness-Number of Transfer Units (ε-NTU) method [25]. These two methods have different purposes and complement each other. Traditionally, the LMTD method focuses on characterising the overall performance of the heat exchanger. By using iterations, performance can be determined by using the inlet and outlet temperatures of the heat source and heat sink, whilst considering the type of heat exchanger and its geometry. This method permits the heat exchanger dimensions to be evaluated and the heat transfer area needed to reach the desired outlet temperatures and duty to be calculated. In essence, this is more useful in design but not for predicting outlet temperatures without knowing the thermal resistance of the heat pipes. On the other hand, the ε-NTU method aims at predicting the performance and the outlet temperatures of the fluids when they are not known. In this case, the geometry of the heat exchanger is fixed, and the user aims at predicting the exhaust temperatures of both heat source and heat sink flows. Even if these methods are widely used, an indication on their accuracy for different types of heat exchangers is valuable. In particular, the case of HPHEs needs to be more thoroughly investigated.

Some studies evaluating the performance of heat exchangers with the LMTD and ε-NTU methods have been conducted and reported in the literature. *Danielewicz* et al. [26] studied the performance of an air to air two-phase closed thermosyphon-based heat exchanger. A tool based on the ε-NTU method was used to predict the overall heat transfer coefficient and effectiveness of the HPHE, but its accuracy has not been reported. The maximum effectiveness of the HPHE exchanger observed was 60%. *Jouhara* et al. [27] theoretically and experimentally studied the behaviour of an air to air HPHE while changing the air flow rate and inclination angle of the system. The ε-NTU predictions were in good agreement with experimental data for HPHE sizing applications. *Brough* et al. [28] developed and validated a TRNSYS model of heat pipe-based heat exchangers. The TRNSYS component for HPHEs based on e-NTU method was developed by Brough et al. The TRNSYS component was validated against experimental results with an accuracy of 4.4% of the heat recovery.

. Similarly, *Noie* et al. [29] used the ε-NTU method to estimate the performance of an air to air thermosyphon based heat exchanger. The maximum effectiveness of the system reported was 65% but the accuracy of the ε-NTU method was not detailed. In their study, *Ramos* et al. [21] investigated the performance of an air to

water HPHE equipped with six thermosyphons. The experimental results have been compared with a theoretical model based on the ε-NTU technique and a Computational Fluid Dynamics (CFD) simulation. Even though the accuracy of the analytical model was not evaluated, the CFD prediction showed an error of less than 15%. When using a similar system with different arrangements for the passes, *Mroue* et al. [22,30] predicted the performance of the HPHE using the LMTD method and compared it with CFD simulations. For an air temperature of 250 °C and a flow rate of 0.14 kg s^{-1}, the effectiveness values obtained were 17%, 27% and 37% for 1, 2 and 3 passes, respectively. *Hua* et al. [31] reported a distributed parameter model using the ε-NTU method to numerically predict the performance of a multi-pass parallel flow condenser. In the case of this parallel flow condenser, the agreement between the theoretical model and the experiments was within a range of $\pm$20%. According to the literature, the effect of changing the number of passes inside the same heat exchanger has hardly been reported. In particular, changing the flow Reynolds number inside a multi-pass HPHE has not been studied in depth. In parallel, despite the wide use of the LMTD and ε-NTU methods to predict the performance of a heat exchanger, the accuracy of these models is rarely evaluated. Furthermore, these methods need to be adapted in the case of HPHEs, as both evaporator and condenser sections must be studied separately. This paper aims at investigating the impact of the number of passes on the heat exchanger effectiveness by changing the number of passes inside the same HPHE. In addition to the experimental results, the LMTD and ε-NTU methods are used to predict the performance of a HPHE. The accuracy of these models is discussed when estimating the performance of a shell-and-tube HPHE.

2. Methodology

2.1. Experimental setup

The HPHE studied is a shell-and-tube type HPHE recovering thermal energy from a hot air stream and transferring it to a water flow. The test parameters of air and water inlet temperatures were selected to simulate the case of waste heat recovery from the hot air exhaust of an industrial process, which can be reused to heat water. 3D drawings of the HPHE studied are presented in Fig. 1.

To transfer the heat from the hot air stream to the water, 51 wickless copper heat pipes, also known as two-phase closed thermosyphons (TPCT), were installed in a staggered arrangement in 6 rows. The heat pipe outer diameter was 12.7 mm. The evaporator section designates the surface in contact with the heat source (air) whereas the condenser section refers to the surface in contact with the heat sink (water). The transition zone between the evaporator and condenser where no heat transfer takes place is known as the adiabatic section. For the HPHE studied, the length of the evaporator, adiabatic and condenser sections are 180 mm, 22 mm and 79 mm, respectively. The working fluid used in the heat pipe was distilled water. To study the influence of the number of passes on the HPHE performance, different arrangement of baffles in the evaporator have been tested in the same HPHE. By incorporating baffles, the number of passes was changed from 1 to 5, thus increasing the Reynolds number of the air stream. The different arrangements of the passes for the evaporator are shown in Fig. 2.

The air passage through the passes is represented by red arrows in Fig. 3.

For this series of tests, four water flow rates (0.010 kg s^{-1}, 0.013 kg s^{-1}, 0.017 kg s^{-1} and 0.020 kg s^{-1}) have been tested for each arrangement of the passes. The air flow rate was maintained constant ($\dot{m}_{air}$ = 29 kg h^{-1} $\pm$7) and so were the inlet temperatures of
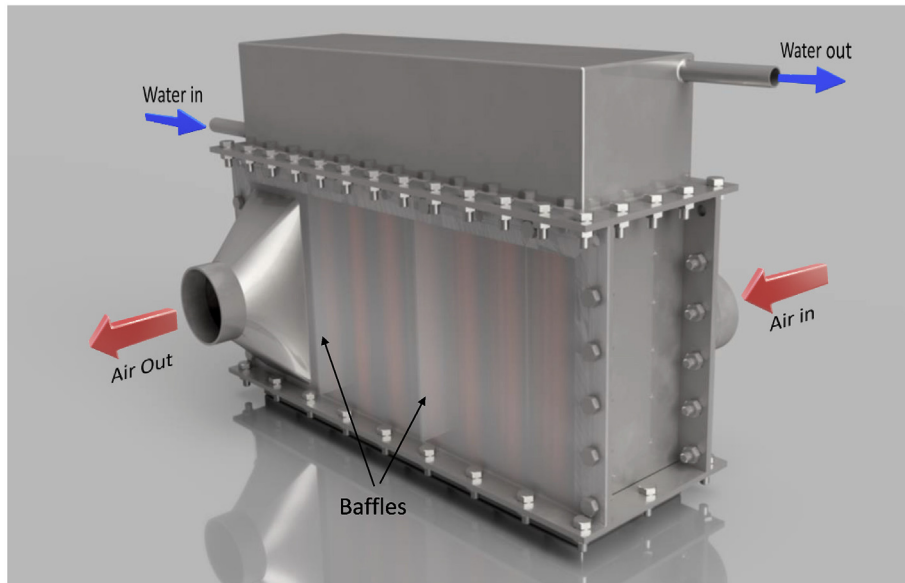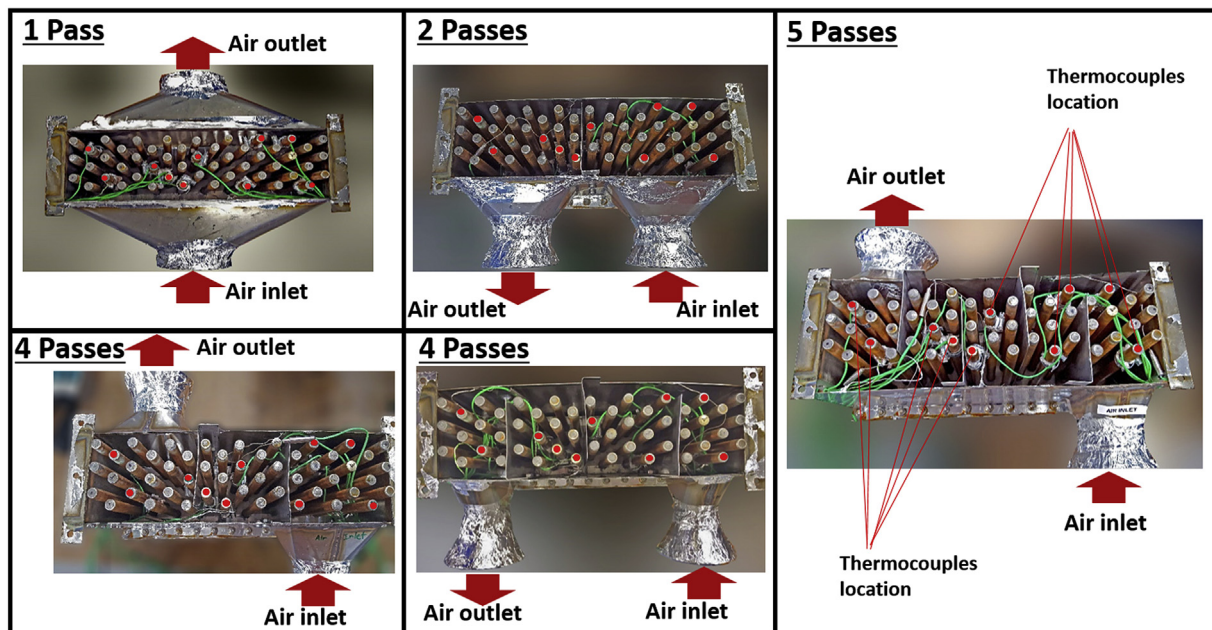
Fig. 1. Drawing of the HPHE studied.

Fig. 2. Arrangement of the passes for the air at the evaporator section of the HPHE.

the air flow ($T_{air, in}$ = 102 °C ± 1) and water flow ($T_{water, in}$ = 15 °C ± 2). The air flow was maintained at a constant temperature by a feedback control system, while the water cooling cycle was an open loop. The experimental conditions are summarized in Table 1.

The temperatures of air and water inlets and outlets and the evaporator and adiabatic section temperatures of the heat pipes were measured using K-type thermocouples. Two thermocouples were used to measure the air temperature at the inlet and outlet of the HPHE, and two thermocouples at the water inlet and outlet. A thermocouple was installed after each air pass in the HPHE, and ten thermocouples were installed on the evaporator section of the heat pipes of the HPHE. The working temperature of ten of the heat pipes, two or more in each pass depending on the number of passes

case, has been recorded.i.e five heat pipes in each pass were measured for the case of two passes, and two heat pipes in each pass were measured for the case of five passes. To measure the air flow rate, an anemometer (Omega FMA900 series) was used while the water flow rate was measured by a turbine flow sensor (Omega FTB370 series). All the sensors were linked to a data logger (MSI Datascan 7320). In the test rig, the HPHE was connected to a closed loop air heat source and an open loop water heat sink. The air loop consisted of a damper, used as a throttle valve to control the air flow rate, a fan, and electrical heaters controlled by a PID system. The electrical power of the heaters was 3 kW due to the electrical supply specifications at the laboratory. The PID controller was used to set a constant value of the air temperature at the inlet of the heat exchanger. As for the open water loop, the flow was controlled by a
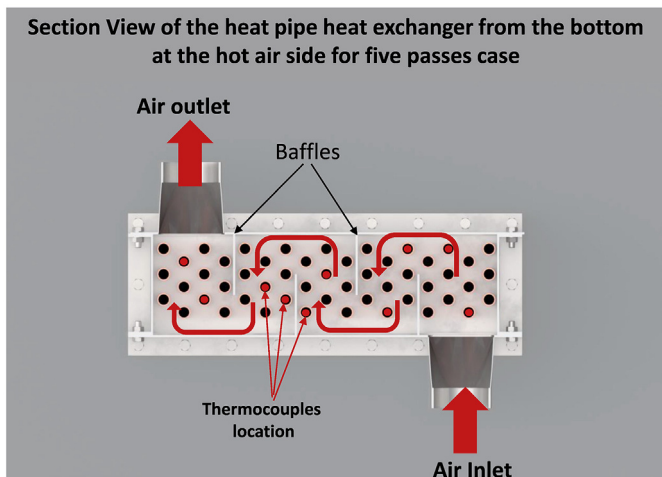
Fig. 3. Air passage through the passes of the HPHE − case of five passes.

water valve. The test rig and piping and instrumentation diagram (P&ID) are presented in Figs. 4 and 5. The fan blows the air through the heaters which heats the air to temperature setpoint which was selected to be 100 °C and measured through a thermocouple installed after the heater. Then, the air passes through the HPHE and cools down and flows through the fan and the cycle is repeated. The closed loop of the air enabled to heat the air to 100 °C using a 3 kW heater and at higher flow rate than an open loop option.

For each experiment, the Reynolds number of the air and water streams are presented in Table 2.

The Reynolds number of the air was higher for 3 passes than 4 due to higher flow air in this experiment.

2.2. Thermal analysis

As briefly introduced, in the analytical investigation of heat exchangers two methods prevail. The LMTD method is used to characterise the performance of a heat exchanger, based on the temperatures of the two fluids at inlet and outlet. This method is

Table 1
Experimental conditions.

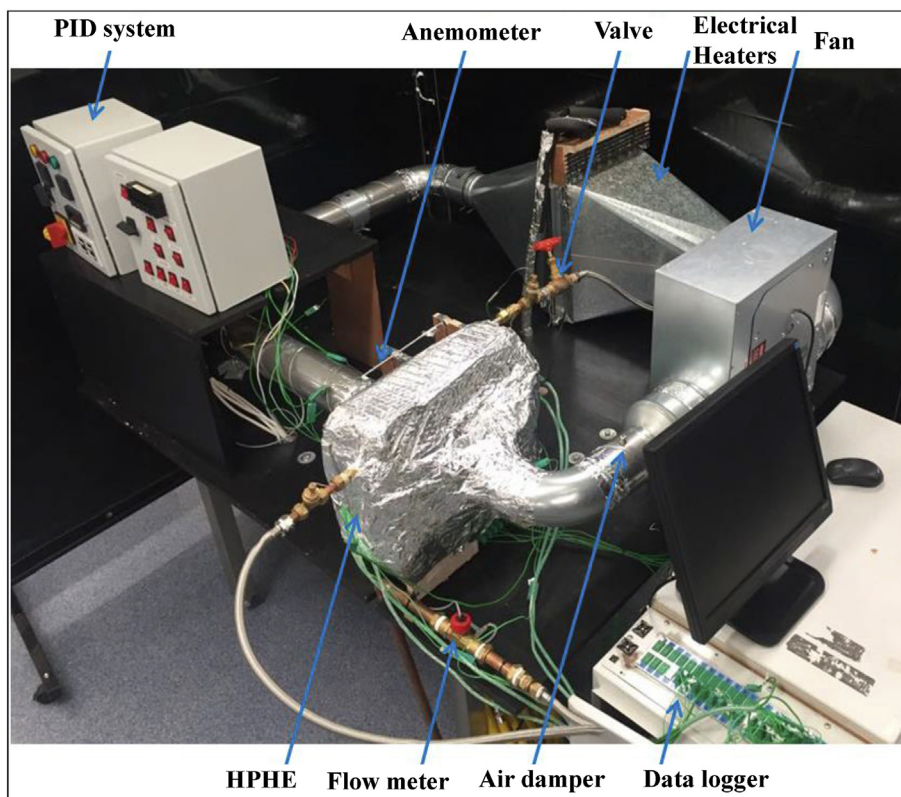| Number of passes	Air		Water		
	Inlet temperature	Mass flow rate	Inlet temperature	Flow rates tested for each number of passes	
	°C	kg.h^{-1}	°C	kg.s^{-1}	kg.h^{-1}
5	102.7	27.8−29.4	14.5−15.6	0.010	35.9
4	102.1	22.8−25.5	14.2−15.3	0.013	48.1
3	101.1	30.2−31.3	14.1−16.8	0.017	61.1
2	102.3	30.7−34.9	13.7−14.8	0.020	71.9
1	102.6	24.4−26.7	16.4−17.0		

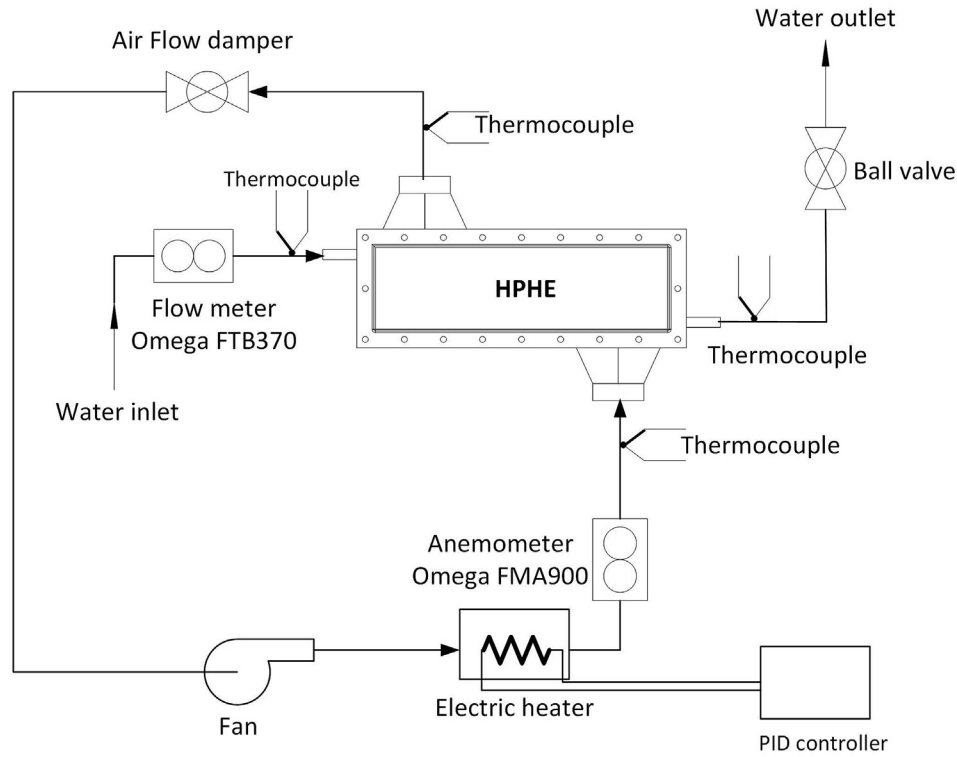

Fig. 4. Test rig of the HPHE.

Fig. 5. Piping and Instrumentation Diagram (P&ID) of the test rig.

Table 2
Air and water Reynolds number for each test.

Number of Passes	Air Flow Reynolds Number	Water Flow Rate (kg.s^{-1})	Water velocity (m/s)	Water Flow Reynolds Number
5	768	0.010	0.0021638	27.4
	813	0.013	0.0028995	35.5
	771	0.017	0.0034621	40.4
	778	0.020	0.0043276	50.2
4	434	0.010	0.0021638	26.5
	472	0.013	0.0028995	34.5
	463	0.017	0.0036135	42.1
	490	0.020	0.0043276	49.4
3	515	0.010	0.0021638	28.0
	515	0.013	0.0028995	34.8
	529	0.017	0.0036785	42.5
	514	0.020	0.0043276	49.6
2	281	0.010	0.0021638	26.4
	296	0.013	0.0028995	34.6
	298	0.017	0.0036135	41.3
	320	0.020	0.0043276	50.2
1	120	0.010	0.0021638	27.0
	112	0.013	0.0028129	33.9
	110	0.017	0.0036135	43.3
	111	0.020	0.0043276	51.9

often used to size a heat exchanger according to the desired outlet temperatures. If the geometry of the heat exchanger is known, the ε-NTU method is also able to predict the performance of the HPHE as represented by the heat transfer rate. Consequently, the outlet temperature of the heat source and heat sink can be determined. In the present study, the design geometry of the heat exchanger is known and the prediction of the overall HPHE performance is investigated. Furthermore, an accurate prediction of the outlet temperature with the ε-NTU method is of interest.

2.2.1. HPHE thermal resistance

Both LMTD and ε-NTU methods are based on the electrical

analogy approach, where the thermal resistance of the heat exchanger is considered as an electrical resistance. Fig. 6 illustrates the electrical resistance diagram of a HPHE.

The HPHE consists of thermosyphons connected in parallel in the diagram, where each thermosyphon is in contact with the hot air stream at the evaporator. Each thermosyphon works independently and transfers heat to the condenser section in contact with the cold water flow. According to the electrical analogy of Fig. 7, the total thermal resistance R_{HPHE} of the HPHE can be calculated as follows [13]:
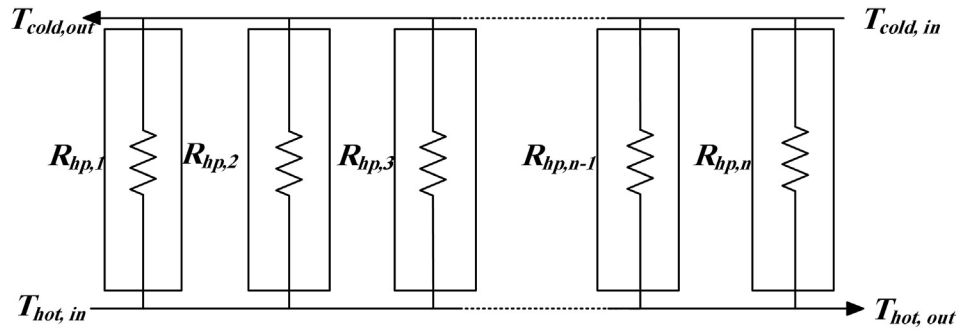
Fig. 6. Electrical-thermal resistance analogy of the HPHE.
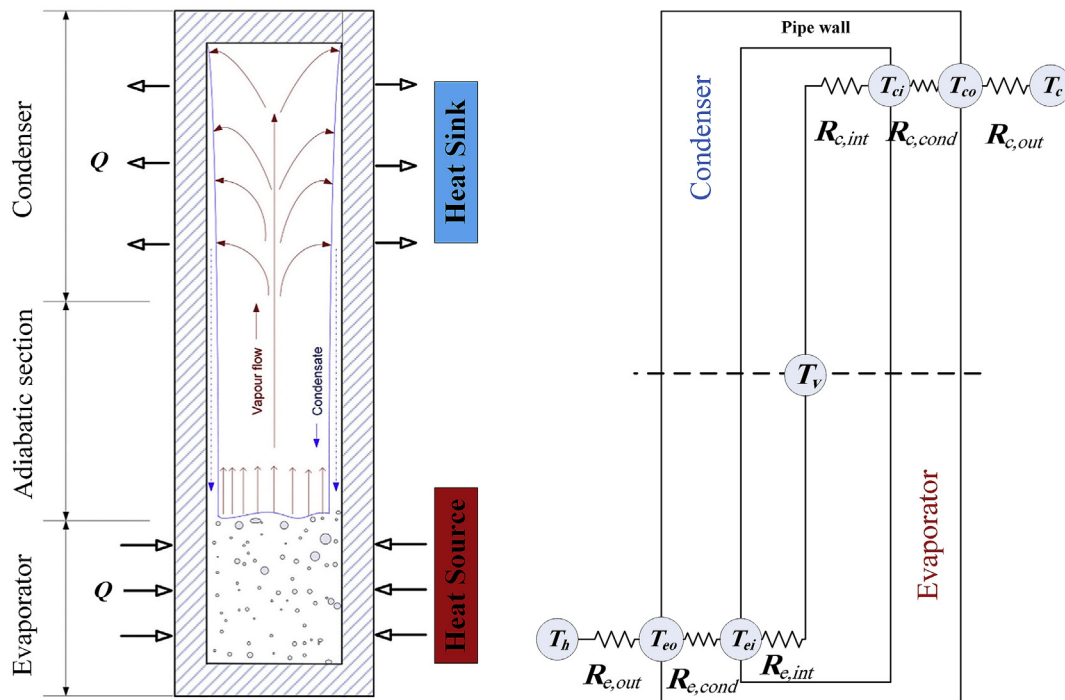

Fig. 7. Two-phase working cycle of a heat pipe and its corresponding thermal resistance model.

$$\frac{1}{R_{HPHE}} = \frac{1}{R_{hp,1}} + \frac{1}{R_{hp,2}} + \dots + \frac{1}{R_{hp,n-1}} + \frac{1}{R_{hp,n}} \qquad (1)$$

where R is the thermal resistance (K.W^{-1}), the subscripts hp refers to heat pipe, and n is the number of heat pipes in the heat exchanger. Assuming that the resistance of a copper thermosyphon is equal for all thermosyphons, the total thermal resistance R_{HPHE} of the heat pipe heat exchanger can be expressed as:

$$R_{HPHE} = \frac{R_{hp}}{n} \qquad (2)$$

with R_{hp} the average resistance of a heat pipe (K.W^{-1}), and n the number of heat pipes in the heat exchanger. To predict theoretically the average resistance of a heat pipe R_{hp}, the working cycle of a thermosyphon must be studied. To transport thermal energy from a heat source to a heat sink, heat pipes use the two-phase cycle of a working fluid. At the location where the heat source is located, the

working fluid inside the heat pipe boils and turns to vapour, thus carrying energy. Driven by the pressure gradient inside the pipe, the vapour rises to the condenser and condenses at the cold wall contact area. The thermal energy is released to the wall and transferred to the heat sink. Finally, the condensate returns to the evaporator section by the action of gravity (thermosyphons) or by capillary action (wicked heat pipes). In the case studied, thermosyphons are used. In accordance with the previously described phase change cycle of a working fluid inside a heat pipe, a thermal resistance analogy of a heat pipe can be made. The two-phase cycle of a thermosyphon and its corresponding thermal resistance model are presented in Fig. 7.

The temperature symbols showin in Fig. 7 are the following: T_h is the hot stream temperature, T_{eo} is the outer wall surface temperature of the evaporator, T_{ei} is the inner wall surface temperature of the evaporator, T_V is the saturation temperature of the heat pipe working fluid at the adiabatic section, T_{ci} is the inner wall surface temperature of the condenser, T_{co} is the outer wall surface temperature of the condenser, and T_c is the cold stream temperature.

The total resistance of a heat pipe R_{hp} can be obtained by Ref. [32]:

$$R_{hp} = R_{e,out} + R_{e,cond} + R_{e,int} + R_{c,int} + R_{c,cond} + R_{c,out} \quad (3)$$

In this model, $R_{e,out}$ and $R_{c,out}$ are the forced convection heat transfer resistances at the evaporator and condenser, respectively. $R_{e,cond}$ and $R_{c,cond}$ represent wall radial conduction at the evaporator and condenser, respectively. $R_{e,int}$ and $R_{c,int}$ correspond to the boiling and condensation resistances of the TPCT (K.W^{-1}), respectively. To estimate the boiling and condensation resistances, the relation between thermal resistance and heat transfer coefficient is:

$$R = \frac{1}{hA} \quad (4)$$

with R being the total overall thermal resistance (K.W^{-1}), h the heat transfer coefficient (W.m^{-2}.K^{-1}), and A the heat transfer surface area (m^2). To predict the heat transfer coefficient for condensation, the *Nusselt* [33] correlation is generally used [34]:

$$h_{condensation} = 0.943 \left[\frac{\rho_l (\rho_l - \rho_v) h_{fg} g k_l^3}{\mu_l L_c (T_V - T_{ci})} \right]^{1/4} \quad (5)$$

where ρ_l and ρ_v are the liquid and vapour densities (kg.m^{-3}), h_{fg} is the latent heat of vaporization (J.kg^{-1}), g is the gravitational acceleration (m.s^{-2}), k_l is the thermal conductivity of the liquid (W.m^{-1}.K^{-1}), μ_l is the liquid dynamic viscosity (Pa.s), L_c is the condenser length (m), T_V is the saturation temperature of the working fluid (K), and T_{ci} is the temperature of the condenser wall (K). To estimate the boiling heat transfer coefficient, the correlation by *Rohsenow* [35] is advised for a wide range of applications [36]:

$$h_{boiling} = \mu_l . h_{fg} \left[\frac{g.(\rho_l - \rho_v)}{\sigma} \right]^{\frac{1}{2}} . \left[\frac{C_P}{\left(C_{sf} . h_{fg} . Pr_l^n \right)} \right]^3 . (\Delta T_{sat})^2 \quad (6)$$

In the correlation by *Rohsenow* [35], μ_l is the liquid dynamic viscosity (Pa.s), h_{fg} is the latent heat of vaporization (J.kg^{-1}), g is the gravitational acceleration (m.s^{-2}), ρ_l and ρ_v are the liquid and vapour densities (kg.m^{-3}), σ is the working fluid surface tension (N.m^{-1}), $Pr = \mu_l C_{P,l}/k_l$ is the liquid Prandtl number, C_P is the specific heat (J.kg^{-1}.K^{-1}), k_l is the thermal conductivity of the liquid (W.m^{-1}.K^{-1}), C_{sf} is a constant depending on the surface-fluid combination, n is a constant depends on the liquid-surface combination which equals to 1 for this study, and ΔT_{sat} is the difference of temperature between the evaporator wall and the saturation temperature of the working fluid $(T_{ei} - T_v)$ (K). The radial conduction resistance of the walls at the evaporator and condenser are expressed respectively by:

$$R_{e,cond} = \ln(D_o / D) / (2\pi L_e k_w) \quad (7)$$

$$R_{c,cond} = \ln(D_o / D) / (2\pi L_c k_w) \quad (8)$$

with D_o being the external diameter of the thermosyphon (m), D being the internal diameter of the thermosyphon (m), k_w is the wall thermal conductivity (W.m^{-1}.K^{-1}), and L_e and L_c are the evaporator and condenser lengths, respectively (m). The forced convection resistance at the evaporator $R_{e,out}$ and condenser $R_{c,out}$ can be expressed in terms of forced convection heat transfer coefficients and the corresponding heat transfer area using **Eq. (4)**. To determine the forced convection heat transfer coefficient of each pipe,

the correlations by *Zukauskas* [19,37,38] can be used:

$$Nu = \frac{h_{forced_{convection}} D_o}{k} = 1.04 Re^{0.4} Pr^{0.36} (Pr/Pr_s)^{0.25} \; for \, Re < 500 \quad (9)$$

$$Nu = 0.71 Re^{0.5} Pr^{0.36} (Pr/Pr_s)^{0.25} \; for \, 500 < Re < 1000 \quad (10)$$

$$Re = \frac{\rho V D_o}{\mu} \quad (11)$$

where Nu is the Nusselt number, $h_{forced_{convection}}$ is the forced convection heat transfer coefficient (W.m^{-2}.K^{-1}), D_o is the external diameter of a TPCT (m), k is the thermal conductivity of the liquid (W.m^{-1}.K^{-1}), Re is the Reynolds number, Pr and Pr_s are the Prandtl number of the flow and the Prandtl number at the surface temperature, respectively, and S_T and S_L the transverse pitch and longitudinal pitch of the staggered heat exchanger (m), respectively. For a number of rows less than sixteen, the Nusselt number obtained by the *Zukauskas* [38] correlations must be corrected by a coefficient F, $Nu_{corrected} = FNu$, as given in Table 3 [19,38]:

In the case studied, the number of rows at the evaporator varies according to the number of passes. The total number of rows for the case of one pass was six, while the total number of rows for the case of two and five passes can be considered 10 and 25, respectively. From the above equations, it can be concluded that the total thermal resistance of the HPHE is influenced by the flow Reynolds number. Thus, according to the theoretical model, a change of mass flow rate or of the hydraulic diameter, leading to a change in Reynolds number, will change the performance of the HPHE. The air velocity increased in the pass due to the decrease of the cross sectional area for the same flow rate. As a result, the Reynolds number increases with the increase of the velocity.

2.2.2. Logarithmic mean temperature difference (LMTD) method

A theoretical model based on the LMTD method was built to predict the performance of the heat exchanger. The total heat transfer rate of the HPHE can be calculated from the following equation:

$$Q = \frac{\Delta T_{LM}}{R_{HPHE}} \quad (12)$$

where Q is heat transfer rate (W), ΔT_{LM} is the logarithmic mean temperature of the inlet and outlet air and water streams, and R_{HPHE} is the total thermal resistance of the HPHE (K.W^{-1}). ΔT_{LM} for a cross flow heat exchanger can be calculated from:

$$\Delta T_{LM} = \left(\frac{(T_{air,in} - T_{water,out}) - (T_{air,out} - T_{water,in})}{\ln \left(\frac{T_{air,in} - T_{water,out}}{T_{air,out} - T_{water,in}} \right)} \right) \quad (13)$$

The thermal energy recovered by the water flow at the condenser is given by the following relation:

Table 3
Correction coefficient, F, for a number of rows less than 16.

Number of rows	1	2	3	4	5	7	10	13
F (staggered)	0.64	0.76	0.84	0.89	0.93	0.96	0.98	0.99

$$Q = \dot{m}_{water} C_{P,water} (T_{water,out} - T_{water,in}) \quad (14)$$

where $\dot{m}_{water}$ is the water mass flow rate (kg.s^{-1}), $C_{P,water}$ is the specific heat of water (J.kg^{-1}.K^{-1}), and $T_{water,in}$ and $T_{water,out}$ are the temperatures of the water at the inlet and outlet of the heat exchanger (K), respectively. A similar analysis of the heat transfer rate can be made by focusing on the air flow. The heat transfer rate can be written as:

$$Q = \dot{m}_{air} C_{P,air} (T_{air,in} - T_{air,out}) \quad (15)$$

where $\dot{m}_{air}$ is the air mass flow rate (kg.s^{-1}), $C_{P,air}$ is the specific heat of air (J.kg^{-1}.K^{-1}), and $T_{air,in}$ and $T_{air,out}$ are the temperatures of the air at the inlet and outlet of the heat exchanger (K), respectively. Theoretically, all the energy recovered from the hot air stream should be transferred to the water. The effectiveness measures the performance of a heat exchanger and is expressed by the ratio of the actual heat transfer rate to the maximum possible heat transfer rate. The maximum heat transfer rate of a counter flow heat exchanger is calculated when either the outlet temperature of the hot fluid reaches the inlet temperature of the cold fluid, or when the outlet temperature of the cold fluid reaches the inlet temperature of the hot fluid. The effectiveness (ε) of the HPHE is given by the following expression [20]:

$$\varepsilon_{HPHE} = \frac{Q_{water}}{Q_{max}} \quad (16)$$

Q_{water} is the actual heat transfer rate recovered (W) and Q_{max} is the maximum possible heat transfer rate (W). The maximum heat transfer rate achievable by a heat exchanger depends on the inlet temperatures of both fluids and on the minimum heat capacity rate of the fluids as follows:

$$Q_{max} = C_{min} (T_{air,in} - T_{water,in}) \quad (17)$$

In this expression C_{min} is the minimum heat capacity rate (W.K^{-1}), and $T_{air,in}$ and $T_{water,in}$ are the inlet temperatures of the air and water streams, respectively. Eq. (17) stipulates that the maximum heat exchange achievable is the case where the fluid with minimum heat capacity reaches the temperature of the other fluid. Indeed, the heat capacity rate indicates the capacity of a fluid to increase its temperature for a given heat transfer rate. In this study, the fluid with minimum heat capacity rate is air. Thus, the minimum capacity rate C_{min} can be written as:

$$C_{min} = \dot{m}_{air} C_{P,air} \quad (18)$$

with $\dot{m}_{air}$ is the air mass flow rate (kg.s^{-1}), and $C_{P,air}$ is the specific heat of water (J.kg^{-1}.K^{-1}). Based on the above equations from the LMTD method, the effectiveness of the heat exchanger can be predicted using the inlet and outlet temperatures of the HPHE.

2.2.3. Effectiveness-Number of Transfer Units (ε-NTU) method

In contrast to the LMTD method, which determines the effectiveness of the HPHE using both inlet and outlet temperatures of the streams, the ε-NTU method allows a prediction of both outlet temperatures and effectiveness of the heat exchanger. As its name indicates, this approach is based on two dimensionless parameters: the effectiveness of the heat exchanger, ε, and the number of transfer units, NTU, defined as [19]:

$$\varepsilon_{HPHE} = \frac{Q}{Q_{max}} = f(NTU) \text{ and } NTU = \frac{UA}{C} \quad (19)$$

U is the overall heat transfer coefficient of the heat exchanger (W.m^{-1}.K^{-1}), A is the heat transfer surface area (m^2) and C is the heat capacity rate (W.$°$K^{-1}). According to this expression, if the effectiveness, ε, of the heat exchanger and the maximum theoretical heat transfer rate are determined, it is possible to estimate the experimental heat transfer, Q, of a system. By using Eq. (17), the maximum heat transfer rate, Q_{max}, can be calculated. Therefore, if the effectiveness, ε, is calculated, by using Eq. (14) and Eq. (15), it is possible to predict the outlet temperature of both air and water streams. Indeed, the core of the ε-NTU technique is the direct evaluation of the heat exchanger effectiveness, ε, which is calculated as a function on the NTUs. To do so, in the case of a HPHE, the evaporator and condenser sections must be studied separately. At the evaporator, thermal energy is transferred by the hot air to the working fluid while at the condenser, the working fluid transfers its thermal energy to the cold water. These two sides can be studied separately. For both sections, the fluid is in a cross-flow configuration with the working fluid inside the heat pipe, with the source and sink fluid directions in counter flow. Therefore, the HPHE studied can be identified as an indirect-transfer-type system, constituted of a first direct type heat exchanger of n_e rows at the evaporator and of a second direct-type heat exchanger of n_c rows at the condenser [39]. Many correlations are reported in the literature to estimate the effectiveness, ε, of different types of heat exchangers [19,40]. In the case of a HPHE, as phase-change occurs inside the heat pipe, the temperature of the working fluid is considered constant when heat is absorbed. Therefore, by definition, its specific heat, c_p, and heat capacity rate, C, approach infinity. As a result, the capacity ratio, $C_r = C_{min}/C_{max}$, is equivalent to zero and the effectiveness of a single row is given by Ref. [19]:

Evaporator:

$$\varepsilon_{e,1\ row} = 1 - \exp(-NTU_e) \text{ with } NTU_e = \frac{U_e A_e}{C_e} \quad (20)$$

❖ Condenser:

$$\varepsilon_{c,1\ row} = 1 - \exp(-NTU_c) \text{ with } NTU_c = \frac{U_c A_c}{C_c} \quad (21)$$

In the above equations, A represents the heat transfer area of one single row (m^2), and C is the average heat capacity rate of the fluids (W.K^{-1}), and U is the overall heat transfer coefficient of the sections considered. To obtain the number of transfer units NTU for each section, UA must be evaluated using forced convection correlations developed from empirical data and can be written as:

❖ Evaporator:

$$U_e A_e = \frac{1}{R_{e,out}} = h_{forced_{convection},e} A_e \quad (22)$$

❖ Condenser:

$$U_c A_c = \frac{1}{R_{c,out}} = h_{forced_{convection},c} A_c \quad (23)$$

The forced convection heat transfer coefficient $h_{forced_{convection}}$ can be calculated using the *Zukauskas* [38] correlations in Eq. (9) and Eq. (10). By using the above two equations, the effectiveness of a

single row at the evaporator and condenser can be predicted. For a number of rows at the evaporator (n_e) and condenser (n_c), the overall effectiveness of each section is given by the ε-NTU correlation for a shell-and-tube heat exchanger of n rows. Once again, as the capacity ratio, C_r, tends to zero in the case of heat pipes, the correlation can be simplified. The overall effectiveness of both sections for n rows can be calculated using the following expressions [19,39]:

❖ Evaporator

$$\varepsilon_{e,n_e} = \frac{\left(\frac{1-C_{r,e}\varepsilon_{e,1row}}{1-\varepsilon_{e,1row}}\right)^{n_e} - 1}{\left(\frac{1-C_{r,e}\varepsilon_{e,1row}}{1-\varepsilon_{e,1row}}\right)^{n_e} - C_{r,e}} \xrightarrow{C_r=0} \varepsilon_{e,n_e} = 1 - \left(1 - \varepsilon_{e,1row}\right)^{n_e}$$

(24)

❖ Condenser:

$$\varepsilon_{c,n_c} = \frac{\left(\frac{1-C_{r,c}\varepsilon_{c,1row}}{1-\varepsilon_{c,1row}}\right)^{n_c} - 1}{\left(\frac{1-C_{r,c}\varepsilon_{c,1row}}{1-\varepsilon_{c,1row}}\right)^{n_c} - C_{r,c}} \xrightarrow{C_r=0} \varepsilon_{c,n_c} = 1 - \left(1 - \varepsilon_{c,1row}\right)^{n_c}$$

(25)

The total heat exchanger effectiveness, ε_{HPHE}, can be determined from the overall effectiveness of the evaporator section, ε_{e,n_e}, and of the condenser section, ε_{c,n_c}, by considering which fluid has the larger heat capacity rate. In the case studied, the fluid with higher heat capacity rate, C, is water at the condenser. Hence, the overall effectiveness of the HPHE is given by Ref. [19]:

$$\text{If } C_c > C_e : \varepsilon_{HPHE} = \left(\frac{1}{\varepsilon_{e,n_e}} + \frac{C_e/C_c}{\varepsilon_{c,n_c}}\right)^{-1}$$

(26)

By using the above detailed equations of the ε-NTU method, the effectiveness of the HPHE has been predicted without using the outlet temperature of the fluids. Finally, by using Eq. (14) and Eq. (15), the outlet temperature of both air at the evaporator and water at the condenser can be predicted.

2.2.4. Return on investment (ROI) calculations

The Return On Investment (ROI) is a performance figure used to evaluate the efficiency of an investment from an economic perspective. The ROI can be determined from the following formula [7]:

$$ROI = \frac{Net\ Profit}{Cost\ of\ Investment} \times 100$$

(27)

and the payback period can be determined from the following formula:

$$ROI = \frac{Cumulative\ Cash\ Flow}{Annual\ Net\ Benefit} \times 12\ (months)$$

(28)

where the cost of investment is the total of the HPHE capital cost and installation cost. The net profit is determined from the equivalent cost of the energy recovered, while considering the parasitic load such as energy consumed by fans and pumps due to the installation of the HPHE.
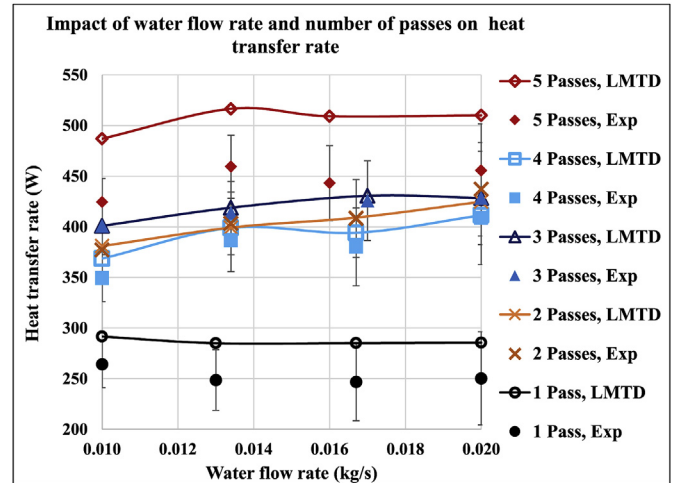

Fig. 8. Impact of water flow rate and number of passes on the total heat transfer rate.

3. Results and discussions

3.1. Impact of the number of passes on the overall heat exchanger performance

The experimental and theoretical heat transfer rates of the HPHE versus the water mass flow rate at different number of passes are presented in Fig. 8. The experimental results are plotted as points while the theoretical results are plotted as lines with points. The experimental heat transfer rate was calculated according to the water stream temperatures and flow rate. The theoretical heat transfer rate was obtained using the LMTD method.

It can be observed that the heat transfer rate of the HPHE increases with the increase in the number of passes. The HPHE achieved up to 264 W of heat recovery for the one pass setup and up to 459 W for the case of five passes. However, despite the efforts made to maintain consistent air and water flow rates and inlet temperatures, a small variation of these factors has played a significant role in the heat recovery in the comparison. For instance, this explains why the amount of heat recovered by the water in the case of four passes is lower than for three passes. It can be noted that heat transfer rate increased with the increase in water flow rate.
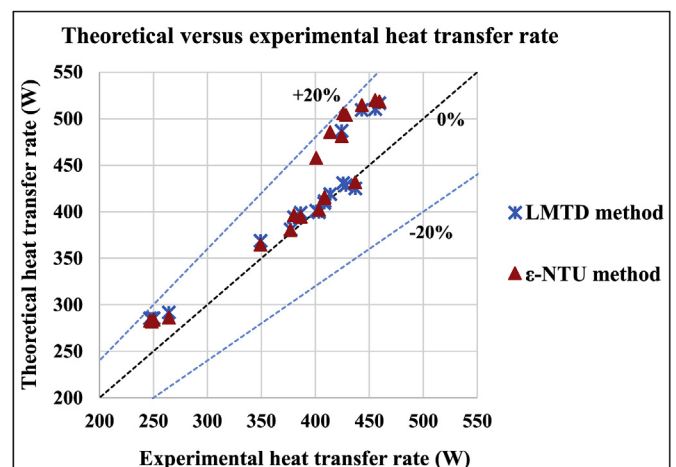

Fig. 9. A comparison between the experimental results and theoretical predictions of heat transfer rate using LMTD and ε-NTU methods.
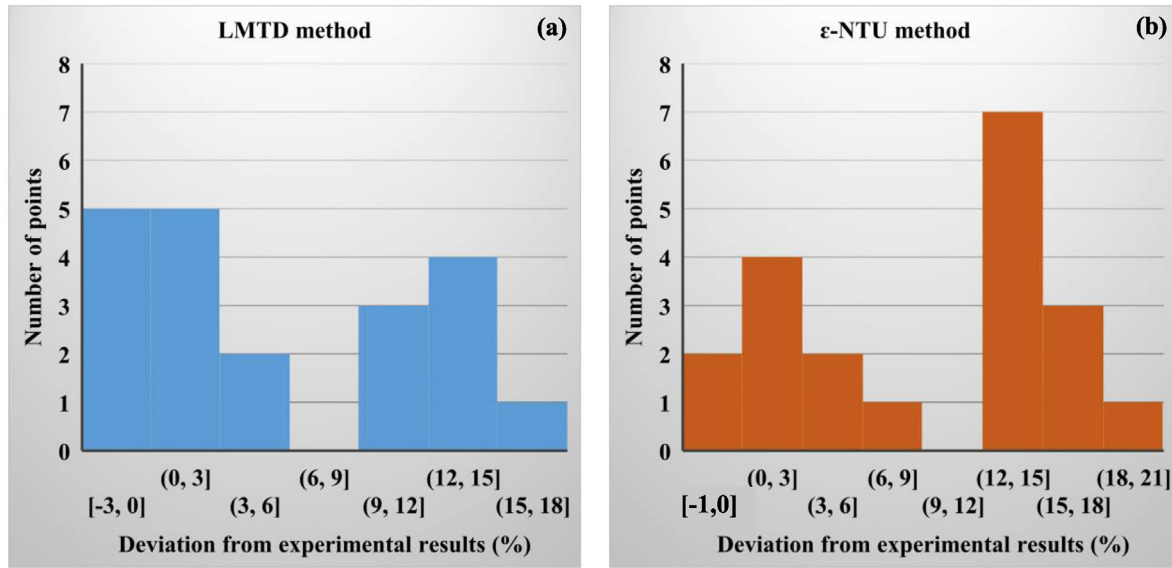
Fig. 10. Histogram of the theoretical predictions deviation from the experimental results of the heat transfer rate: (a) using the LMTD method, (b) using the ε-NTU method.

Moreover, the theoretical predictions using the LMTD model showed a good agreement with the experimental results, although it over-predicted the heat transfer rate for most of the experimental cases. Fig. 9 shows a comparison between the theoretical predictions using the LMTD and ε-NTU methods, versus experimental results of the heat transfer rate. The heat transfer rate was predicted within an error of ±15.5% using the LMTD method and ±19% using the ε-NTU method. The deviation of the theoretical predictions from the experimental results is due to the uncertainty with the experimental results and the accuracy of the heat transfer correlation used to predict the thermal performance of the HPHE. Fig. 10 presents a histogram of the number of points versus the deviation of the predicted results from the experimental results using the LMTD and ε-NTU methods. As Fig. 10 illustrates, the LMTD method had higher accuracy and less error than ε-NTU method. The LMTD method had 10 out of 20 measurement points within an error of ±3% and five points of an error between 12% and 16%. The ε-NTU method had eight measurement points within an error range

of −1% and 6%, seven points in the range of 12% and 15%, and four points in the range between 15% and 20%. In comparison between the two methods, the LMTD had a smaller error range with the majority of the points in the error range of ±6%, while ε-NTU had larger error range up to 20% with over half of the points in the range between 12% and 20%. The LMTD method was more accurate since it evaluates all the thermal resistances but it is more complex, while ε-NTU is simpler to be applied to predict the thermal performance without the complications of the heat pipe two-phase heat transfer.

Fig. 11 illustrates the influence of water mass flow rate on the total effectiveness of the HPHE for the experimental results and the results obtained by the LMTD method at different number of passes. The experimental and theoretical results obtained through ε-NTU method are presented in Fig. 12.

The analysis of the HPHE effectiveness is important as it balances the relative impacts of Reynolds number and variations in flow rates.

From Fig. 11, it can be deduced that the total effectiveness of the HPHE has been improved between number of passes from 1 to 5 by
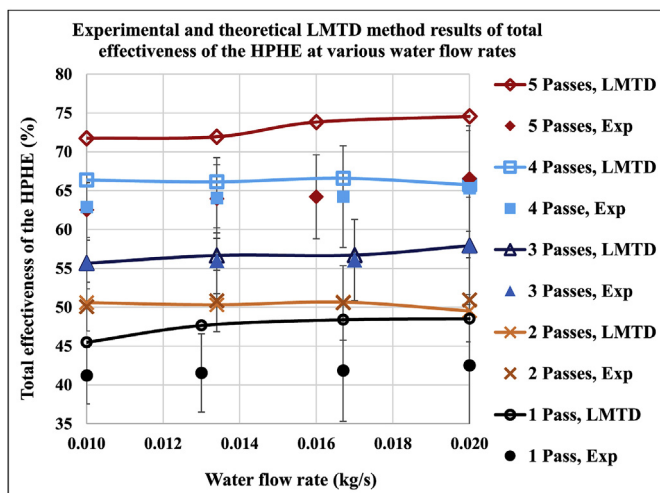

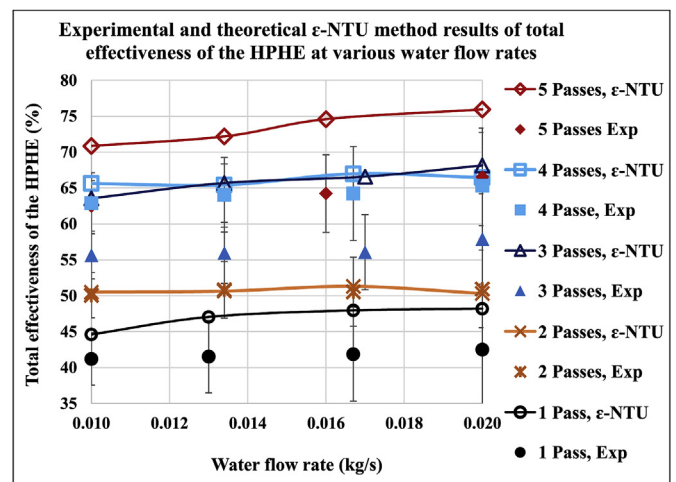**Fig. 11.** Experimental and LMTD method predictions of the total effectiveness of the HPHE.

Fig. 12. Experimental and ε-NTU method predictions of the total effectiveness of the HPHE.

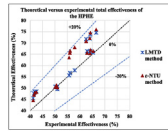**Fig. 13. A comparison between the experimental results and theoretical predictions of the HPHE total effectiveness using the LMTD and ε-NTU methods.**

more than 50%, relative to the effectiveness for one pass. Indeed, by increasing the air Reynolds number from $Re \approx 110$ to $Re \approx 775$, the total HPHE effectiveness increased from 43% to 67%. Moreover, it can be observed that the total effectiveness obtained experimentally was significantly improved between the case of a single pass and that for 4 passes cases, while there was no significant change in experimental results between the case of 4 passes and that for 5 passes. This was due to the higher air mass flow rate for the latter. Both the LMTD and ε-NTU over-predicted the total effectiveness of the HPHE for most of the experimental cases.

The deviation of the theoretical predictions using the LMTD and ε-NTU methods versus the experimental results of the total effectiveness of the HPHE is presented in Fig. 13. The theoretical predictions made with the LMTD method show a very good agreement with the experimental results. For the cases from 1 to 5 passes, the maximum differences between the LMTD prediction and the experimental data were 15.5%, 1%, 1.2%, 5.55%, and 14.9%, respectively. The variations for the cases of one and five passes can be attributed to the fact that the air flow through the pipes in the experiment was not uniform as considered in the theoretical modelling. Overall, the predictions made by the LMTD method are expected to be more accurate as they rely on both inlet and outlet temperatures of the fluids.

As for the ε-NTU model, the performance predictions have been noted to be less accurate, in comparison to the LMTD method. This is to be expected as this method is more theoretical and predicts the performance of the HPHE by considering only the inlet parameters and the geometry of the system. Nevertheless, the maximum error made by the ε-NTU model was only 19% for a number of passes of 3 as shown in Fig. 13. Fig. 14 presents a histogram of the number of points of the predictions versus the

percentage deviation from the experimental results for the LMTD and the ε-NTU methods. The outcome is similar to the heat transfer rate deviation range as the total effectiveness was based on the experimental or theoretical heat transfer rate divided to the maximum heat transfer rate possible. The LMTD method had 12 points out of 20 in the error range less than 6% and seven points in the deviation range between 9% and 15%. However, the ε-NTU method exhibited eight points in the deviation range between −1% and 6%, seven points in the range between 9% and 15%, and four points in the range between 15% and 20%. The LMTD method exhibited more accuracy in comparison with ε-NTU method with more data points closer to the experimental results. The ε-NTU tended to overpredict the results more than the LMTD method.

From this study, it is concluded that the ε-NTU model is more sensitive to the prediction of the forced convection resistance than the LMTD method. Indeed, as shown in Table 2, for three passes, the Reynolds number is calculated to be higher than for four passes, based on the air flow rate measurements. The potential measurement error made on the air flow rate, and thus on the calculation of the Reynolds number at the evaporator, had a direct impact on the prediction by the ε-NTU model. In addition, in the case of three passes, the Reynolds number was higher than $Re = 500$, which indicates that another forced convection correlation could be used to improve the accuracy of the prediction. According to the literature, the accuracy of the semi-empirical forced convection correlations by *Zukauskas* [38] is estimated between 15% and 20% [20].

Other factors may also be responsible of the variations observed in the above results. At first, the air flow and the inlet air temperatures between the experiments varied slightly. A direct impact of these factors on the heat transfer can be expected. Furthermore, the water inlet temperature may vary as well. This partially explains why, at a water flow rate of 0.010 kg/s, the water outlet temperature was more important higher for 3 passes configuration than in the 4 passes configuration Finally, the error associated with the instrumentations used (thermocouples, anemometer, turbine flow sensor, data logger) are also impacting the accuracy of the results, as discussed in Section 3.7.
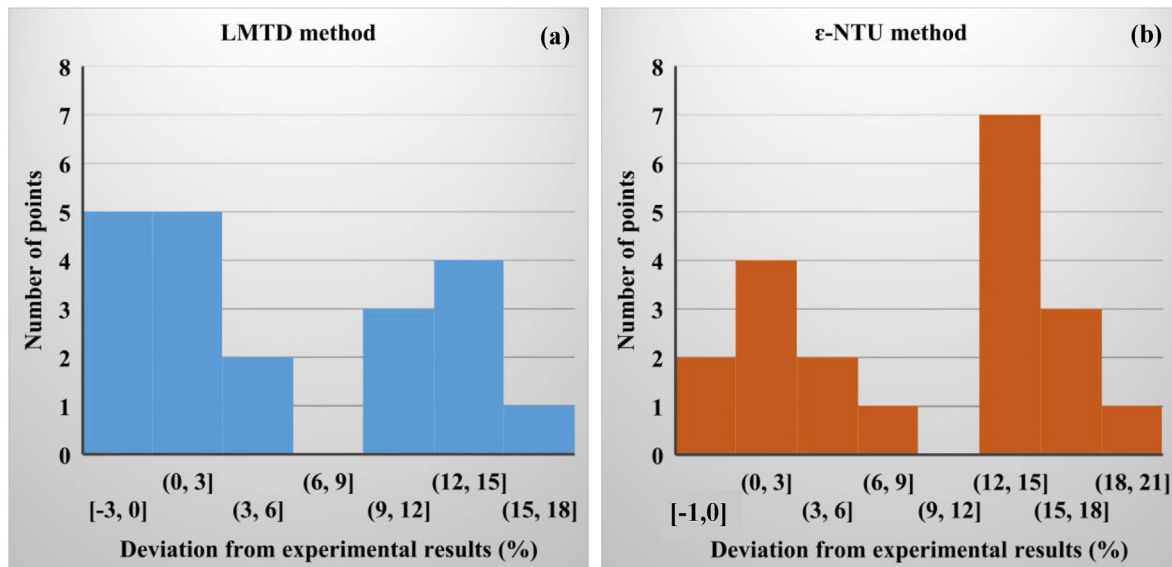

Fig. 14. Histogram of the theoretical prediction deviation from the experimental results of the HPHE effectiveness: (a) using the LMTD method, (b) using the ε-NTU method.
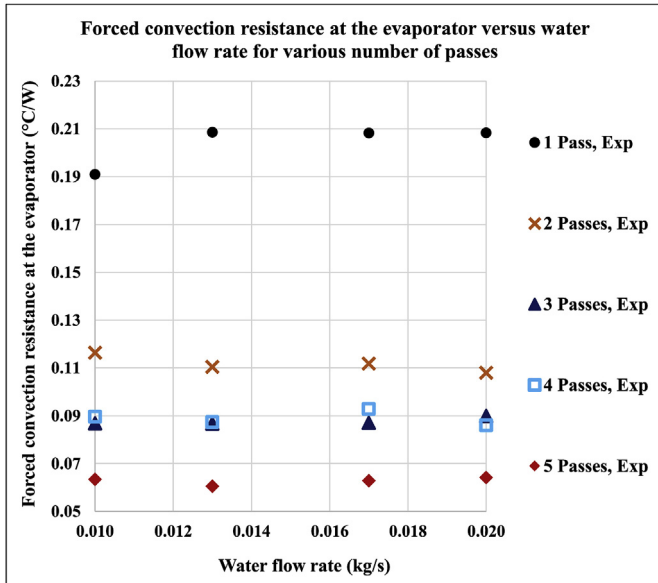
Fig. 15. Forced convection resistance at the evaporator versus water flow rate for various number of passes.

3.2. Impact of the number of passes on the heat transfer resistance at the evaporator

This section focuses on the evaporator section to give detail on the influence of the number of passes on the HPHE performance previously observed. By changing the number of baffles inside the system, the Reynolds number of the air stream varied, which is expected to have a significant impact on the forced convection heat transfer resistance at the evaporator. The impact of the number of passes on the evaporator forced convection resistance is studied in Fig. 15.

Due to the uncertainty in the accuracy and sensitivity of the anemometer used to measure the air flow associated with the air temperature change, the forced convection resistance has been calculated from the energy balance using **Eq. (12)**, based on the
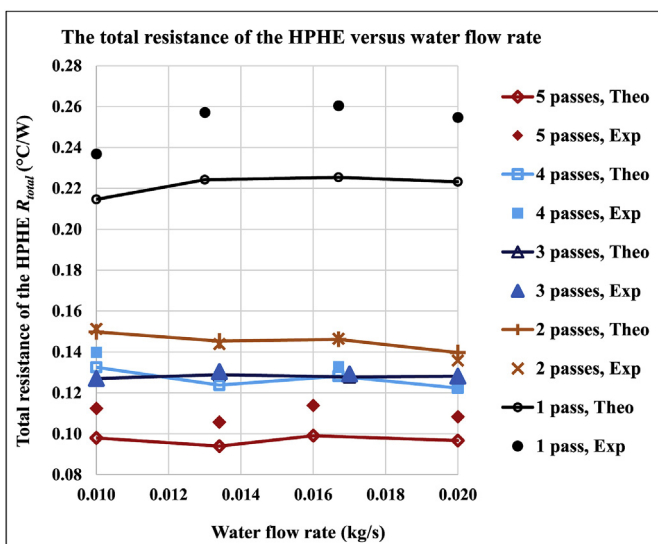

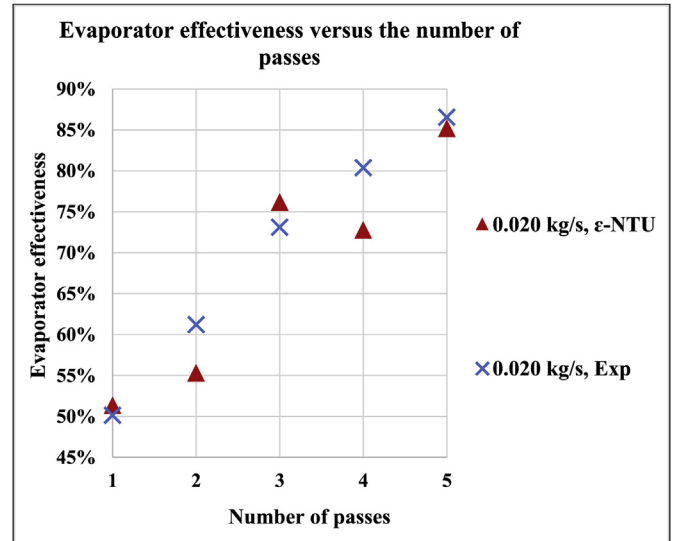**Fig. 16.** The total resistance of the HPHE versus water flow rate.

Fig. 17. Impact of the number of passes on the evaporator effectiveness.

energy gained by water. It was assumed that there was no heat loss to the ambient since the heat exchanger was fully insulated. It has been observed that the higher the number of passes, the lower the forced convection resistance at the evaporator due to the increase in Reynolds number. By using 5 passes instead of 1 for the same heat exchanger, the evaporator thermal resistance was reduced by 70%. This decrease in the evaporator thermal resistance is conveyed to the overall thermal resistance of the HPHE as shown in Fig. 16.

A similar trend in the total thermal resistance of the HPHE with the decrease in the evaporator thermal resistance is observed. This validates the conclusion that the increase in heat recovery is mainly due to the decrease in the evaporator convection thermal resistance and that other factors did not significantly contribute to the increase in the HPHE performance. In addition, it can be noted that the water flow rate had a limited impact on the thermal resistance of the evaporator. The experimental and theoretical effectiveness of the evaporator versus the number of passes in the HPHE is presented in Fig. 17.

For clarification, this analysis is conducted only for a water flow rate of 0.020 kg s^{-1} as the results are similar from one water flow rate to another. From Fig. 17, it can be concluded that a decrease in the evaporator thermal resistance, as the number of passes increased, resulted in an increase in the evaporator effectiveness. Indeed, from 1 to 5 passes, the experimental effectiveness of the evaporator increased from 50% to 87%. The predictions made with the ϵ-NTU method are in good agreement with the experimental data with a maximum error of 9.6%.

By increasing the number of passes, it was observed that the heat transfer coefficient at the evaporator section was improved. As the air passage section is reduced, the Reynolds number increased, and the flow becomes more turbulent. Therefore, the heat transfer rate from the hot air stream to the heat pipes is substantially enhanced.

3.3. Heat transfer at each pass

In this section, only the case in which the HPHE comprised five passes is studied. The objective is to investigate the heat transfer rate at each pass and the air temperature after each pass. For this analysis, a water flow of 0.02 kg s^{-1} has been selected. The air temperature after each pass and the heat transfer rates achieved at
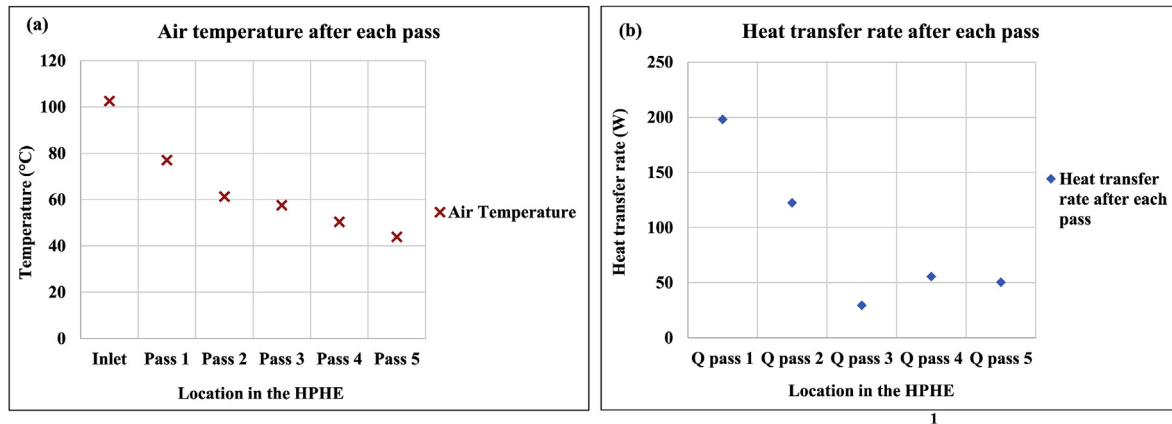
Fig. 18. Experimental results of each pass for 5 passes and water flow rate of 0.02 kg s^{-1} (a): Air temperature trend, (b): Heat transfer rate.

each pass are presented in Fig. 18.

It can be observed that the decrease in air temperature through the HPHE is not linear with the number of passes. Indeed, the heat transfer is much higher for the first passes, which leads to higher differences of temperature inside these passes. The non-linearity of the temperature distribution inside the HPHE justifies the use of the LMTD method in the analysis. In the case of a geometry with five passes, it can be noted that the heat transfer rate at the last pass (Pass 5) is a quarter of the heat transfer rate occurring at the first pass (Pass 1) which is about 50 W against 200 W. Furthermore, the analysis permits one to identify a potential inaccuracy in the temperature measurement in the case of the third pass. An inaccuracy in the temperature measurement at the third pass and fourth pass may have caused the observable discrepancy. This inaccuracy can be due to a non-uniform air distribution between the pipes after each bend, and the position of the air thermocouples.

3.4. Impact of the thermal performance of the HPHE

As previously mentioned, the water flow rate at the condenser did not have any noticeable impact on the forced convection resistance at the evaporator. However, it can be observed in Figs. 8, Figure 11, and Fig. 12 that the water flow rate has a small effect on the overall performance of the HPHE. The influence of the water flow rate on the overall performance of the HPHE has been investigated further. From the previous sections, it can be noted that the heat transfer rate and effectiveness of the HPHE slightly increased with the water flow rate. Between a water flow rate of 0.010 kg s^{-1} and a water flow rate of 0.020 kg s^{-1}, the maximum increase of the HPHE effectiveness was obtained with a geometry of five passes. In this case, increasing the water flow rate from 0.010 kg s^{-1} to 0.020 kg s^{-1} increased the heat transfer rate from 424 W to 456 W. As for the total effectiveness of the HPHE, an increase from 63% to 67% was observed as the flow rate increased from 0.010 kg s^{-1} to 0.020 kg s^{-1}. In comparison, for a constant water flow rate of 0.020 kg s^{-1}, increasing the number of passes from 1 to 5 improved the total effectiveness of the HPHE from 43% to 67%. Hence, within the tested range of water flow rates, it is concluded that the water flow rate has a much lower impact on the performance of the HPHE in comparison to the number of passes.

3.5. Temperature predictions

By using the LMTD model, the average working temperatures of the heat pipes have been predicted and compared with experimental data. The experimental working temperature is the average
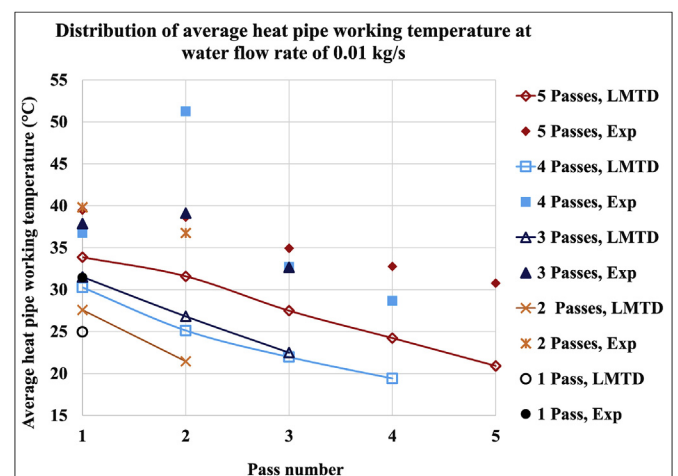

Fig. 19. Average working temperature of heat pipes and LMTD predictions for each pass at a water flow rate of 0.010 kg s^{-1}.

of the temperature measured using the thermocouples placed in the adiabatic section for each pass. The theoretical working temperature was determined through the thermal model by using the two-phase heat transfer correlations presented in the thermal analysis section and considering the heat transfer rate of each heat pipe. The average working temperature of the heat pipes in each row is displayed in Fig. 19. Obviously, depending on the geometry tested and the number of passes in the HPHE, the measurements can only cover the full range of the number of passes inside the tested system. For instance, no working temperatures of the heat pipes in rows number 4, 5 are available when the geometry tested comprises three passes due to the positions of the thermocouples placed on the heat pipes. The average working temperatures of the thermosyphons reported in Fig. 19 were obtained with a water flow rate of 0.010 kg s^{-1}.

The pass number sequence starts from the air inlet to the air outlet. It can be noted that the experimental measurements were higher than the theoretical predictions made with the LMTD method. This could be due to the axial wall conduction in the copper tubes, which was not considered in the theoretical modelling. There is a tendency for the working temperature of heat pipes to be higher at a higher number of passes inside the system. However, experimental data were affected by the inlet temperatures of both air and water streams, which were not rigorously the
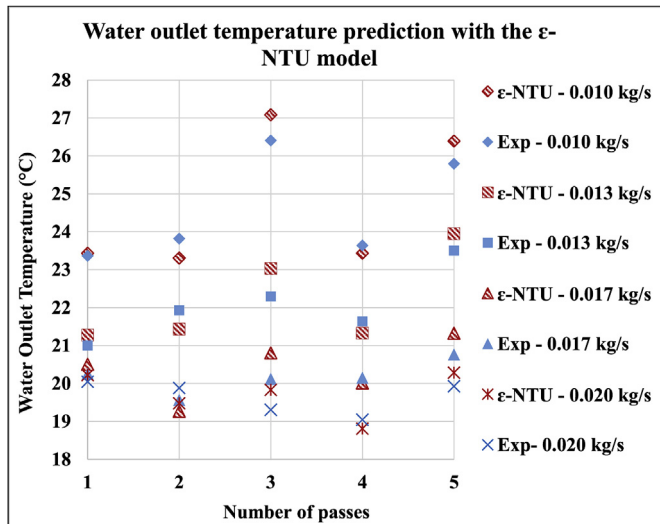
Fig. 20. Experimental water outlet temperature and LMTD predictions.

same for the experiments conducted. The experimental results were obtained from average temperatures of multiple heat pipes. The heat pipe temperature is significantly influenced by its position in the pipe pattern and its exposure to the air flow, which was not uniform. Finally, it can be concluded from Fig. 19 that the working temperature of the heat pipes decreases for successive passes. As the air temperature decreases inside the HPHE due to the heat exchange with the water, the equilibrium working temperature of the thermosyphon decreases accordingly.

As introduced, one of the main advantages of the ε-NTU method is the prediction of the outlet temperatures of the fluids. In Fig. 20, the predictions of the model based on the ε-NTU method are compared with the experimental water outlet temperatures.

Consistent with the preceding analysis, the water outlet temperature increases with the number of passes inside the HPHE. Again, depending on the water inlet temperature, the temperature may fluctuate. Hence, for three passes inside the HPHE, the water outlet temperature was high due to a high water inlet temperature, as shown in Table 1. Nevertheless, it can be claimed that the predictions of the ε-NTU method were quite accurate considering the high specific heat capacity of water. Indeed, based on the HPHE geometry and on the inlet temperature of both streams, the model predicted the water outlet temperatures with a maximum error of ±0.7 °C. It should be noted that for the air outlet temperature, the error in the prediction can reach 9 °C when the error in predicting the heat transfer rate is about 20%. This is due to the low specific heat capacity of air and the low air flow rate during the tests.

3.6. Industrial and economic impact

It was observed from the results that the heat recovery increased by about 74% for the case of the HPHE having 5 passes in comparison with the single pass case. Thus, the HPHE can recover 74% of waste heat in an industrial application during a whole working year, assuming the thermal performance enhancement of the full scale is the same as for the lab scale. Assuming the full scale heat recovery is 100 kW for a single pass, there are 8440 working hours per year and capital and installation costs are £120,000 in total, the pay-back period of the HPHE will be 34 months. The payback period falls into the favourable industrial applications is generally three years or 33% as ROI.

For the case where the HPHE is modified to have 5 passes and

assuming the enhancement of the heat recovery is 74% as for the lab-scale, the payback period is reduced to 24 months for the same setup.

In more detail, the reduction in the payback period came from the fact that the HPHE with a single pass can save £24,150 per annum, while for 5 passes the HPHE case can save roughly £42,000 per annum. These results were based on the saving of natural gas which would be used to generate the heat at a cost of 0.025 £.kWh^{-1} [41].

This study is based on the condition that air mass flow rate and pressure drop of the HPHE for all the cases are equal. However, the hydraulic resistance of the HPHE and pressure drop of the single pass HPHE are less than for 5 passes. Hence, the fan requires more power to compensate for the increased hydraulic resistance in the air duct, and to achieve the same flow rate in a full-scale application. However, the increased parasitic load of the fan which was assumed to be 10 kW will be much less than the increase in the heat recovery which keeps the 5 passes case of the HPHE more efficient and economical. Moreover, the heat recovery and the effectiveness were significantly for the same footprint of the HPHE, which presents a viable solution for limited installation space.

3.7. Uncertainties associated with the experimental results

The main source of uncertainty associated with the experimental heat recovery and effectiveness values came from measurements of temperature and flow rate. The uncertainty associated with the readings of the temperature is (0.05% reading ± 0.38 °C), while the one associated with the water flow meter is ±1% of the full scale. The uncertainty associated with the instruments is listed in Table 4. The propagation of uncertainty associated with experimental heat recovery can be calculated using Equation (29) according to Taylor [42]:

$$S_Q = Q_{out} \times \sqrt{\left(\frac{S_{\dot{V}}}{\dot{V}}\right)^2 + \left(\frac{S_{(T_{water,out} - T_{water,in})}}{(T_{water,out} - T_{water,in})}\right)^2} \quad (29)$$

where $S_{(T_{water,out} - T_{water,in})}$ is the uncertainty associated with the difference in temperature, and $S_{\dot{V}}$ is the uncertainty associated with the water flow rate. The error associated with temperature difference between the water inlet and outlet is:

$$S_{(T_{water,out} - T_{water,in})} = \sqrt{S_{T_{water,out}}^2 + S_{T_{water,in}}^2} \quad (30)$$

The error associated with the effectiveness can be calculated from:

$$S_\varepsilon = \varepsilon \times \sqrt{\left(\frac{S_{Q_{out}}}{Q_{out}}\right)^2 + \left(\frac{S_{Q_{max}}}{Q_{max}}\right)^2} \quad (31)$$

$$S_{Q_{max}} = Q_{max} \times \sqrt{\left(\frac{S_{\dot{V}_{air}}}{\dot{V}_{air}}\right)^2 + \left(\frac{S_{(T_{air,in} - T_{water,in})}}{(T_{air,in} - T_{water,in})}\right)^2} \quad (32)$$

The maximum error associated with the experimental heat

Table 4
Uncertainty associated with instruments used to measure the experimental data.

Parameter	Sensor	Uncertainty
Temperature	Datascan 7320	0.05% ± 0.38 °C
Air velocity	Omega FMA900	±1% of reading
Water flow rate	Omega FTB370	±1% of reading

Table 5
Maximum errors associated with the experimental heat transfer rate.

Heat transfer rate, Q_{out}(W)	Absolute maximum error, S_Q(W)	Maximum relative error $\frac{S_Q}{Q_{out}}$(%)
424.43	23.39	5.51
459.37	31.14	6.78
443.16	37	8.35
455.57	46.14	10.13
349.28	23.25	6.66
386.53	31.02	8.03
380.2	38.53	10.13
408.64	46.07	11.27
400.93	23.37	5.83
413.83	31.06	7.51
425.79	39.25	9.22
428.45	46.09	10.76
377.11	23.29	6.18
403.37	31.04	7.70
408.24	38.53	9.44
437.06	46.12	10.55
264.28	23.16	8.76
248.55	29.99	12.07
246.79	38.47	15.59
250.25	46.05	18.40

Table 6
Maximum errors associated with the experimental effectiveness of the HPHE.

Effectiveness, ε	Absolute maximum error, S_ε	Maximum relative error $\frac{S_\varepsilon}{\varepsilon}$(%)
0.625	0.0353	5.64
0.6395	0.044	6.89
0.6422	0.0542	8.43
0.6656	0.0679	10.20
0.6289	0.0425	6.76
0.6407	0.052	8.11
0.6424	0.0656	10.21
0.6533	0.0741	11.34
0.5567	0.0331	5.95
0.5597	0.0426	7.60
0.5607	0.0521	9.30
0.5791	0.0627	10.83
0.5007	0.0315	6.29
0.5082	0.0396	7.79
0.5055	0.0481	9.51
0.5094	0.0541	10.62
0.412	0.0365	8.85
0.4153	0.0504	12.13
0.4185	0.0654	15.64
0.4251	0.0784	18.44

transfer rate and the total effectiveness of the HPHE are shown in Table 5 and Table 6, respectively.

4. Conclusion

In this study, the performance of an air to water HPHE was investigated theoretically and experimentally. The HPHE was studied at various Reynolds numbers of the air and water flows. The Reynolds number was changed by adding baffles inside the given heat exchanger at the air side and by changing the water mass flow rate.

It was observed from the experimental results that the number of passes had a significant impact on the heat recovery. The enhancement of the HPHE thermal performance was due to the enhancement of the heat transfer coefficient by forced convection at the air side. The forced convection resistance at the evaporator has been reduced by more than 70% by increasing the Reynolds number of the air flow.

The heat recovery increased from 264 W to 459 W, which represents a 74% increase. The heat recovery increased from 264 W to 459 W, which represents a 74% increase. The enhanced heat recovery led to increase the effectiveness of the HPHE from 43% for a single pass to 67% for five passes. The maximum effectiveness enhancement by increasing the number of passes was 56%. However, the increase of the water flow rate had less impact on the heat recovery and the total effectiveness of the HPHE.

Furthermore, two theoretical models based on the LMTD method and the ε-NTU method have been developed to predict the thermal performance of the HPHE, and compared with experimental data. The LMTD method, which used the inlet temperatures of the fluids and geometry of the HPHE, predicted the performance of the HPHE to within ±15.5% error. However, the ε-NTU model prediction showed an error up to 19%. Yet, the ε-NTU method permits a prediction of the performance when the outlet temperatures of the fluids are unknown and is simpler to be applied. Moreover, the ε-NTU model predictions of the outlet temperatures of both air and water streams were with an accuracy of ±0.7 °C. It was also observed that the ε-NTU model was more influenced by the uncertainty of the measurements on the air flow than the LMTD model, which relies more on temperature measurements.

The LMTD model was used to predict the working temperature of the heat pipes which showed an overprediction of 8 °C, the accuracy could be further enhanced in future studies by investigating different two-phase heat transfer correlations.

Both modelling tools can be applied to predict the thermal performance of a HPHE where the LMTD method consider the two-phase heat transfer in the heat pipe while ε-NTU offers a simplified approach with less accuracy assuming that the heat pipes are fully functional.

This study presented a multi-pass solution which enhances the effectiveness and the heat recovery of the HPHE for the same footprint and overall dimensions, which is desirable when the available space for installation is limited in industrial applications.

Declaration of competing interest

The authors declare that they have no known competing financial interests or personal relationships that could have appeared to influence the work reported in this paper.

Acknowledgements

References

[1] Mokkapati V, Lin C-S. Numerical study of an exhaust heat recovery system using corrugated tube heat exchanger with twisted tape inserts. Int Commun Heat Mass Tran 2014;57:53—64. https://doi.org/10.1016/J.ICHEATMASSTRANSFER.2014.07.002.
[2] Jouhara H, Meskimmon R. Experimental investigation of wraparound loop heat pipe heat exchanger used in energy efficient air handling units. Energy 2010;35:4592—9. https://doi.org/10.1016/j.energy.2010.03.056.
[3] Noie-Baghban SH, Majideian GR. Waste heat recovery using heat pipe heat exchanger (HPHE) for surgery rooms in hospitals. Appl Therm Eng 2000;20:1271—82. https://doi.org/10.1016/S1359-4311(99)00092-7.
[4] Delpech B, Axcell B, Jouhara H. Experimental investigation of a radiative heat pipe for waste heat recovery in a ceramics kiln. Energy; 2018. https://doi.org/10.1016/j.energy.2018.12.133.
[5] Egilegor B, Jouhara H, Zuazua J, Al-Mansour F, Plesnik K, Montorsi L, et al. ETEKINA: analysis of the potential for waste heat recovery in three sectors: aluminium low pressure die casting, steel sector and ceramic tiles manufacturing sector. Int J Thermofluids 2019:100002. https://doi.org/10.1016/j.ijft.2019.100002.
[6] Delpech B, Milani M, Montorsi L, Boscardin D, Chauhan A, Almahmoud S, et al. Energy efficiency enhancement and waste heat recovery in industrial processes by means of the heat pipe technology: case of the ceramic industry. Energy 2018;158:656—65. https://doi.org/10.1016/j.energy.2018.06.041.

[7] Brough D, Mezquita A, Ferrer S, Segarra C, Chauhan A, Almahmoud S, et al. An experimental study and computational validation of waste heat recovery from a lab scale ceramic kiln using a vertical multi-pass heat pipe heat exchanger. Energy 2020:118325. https://doi.org/10.1016/j.energy.2020.118325.

[8] Almahmoud S, Jouhara H. Experimental and theoretical investigation on a radiative flat heat pipe heat exchanger. Energy 2019;174:972−84. https://doi.org/10.1016/j.energy.2019.03.027.

[9] Jouhara H, Almahmoud S, Chauhan A, Delpech B, Bianchi G, Tassou SA, et al. Experimental and theoretical investigation of a flat heat pipe heat exchanger for waste heat recovery in the steel industry. Energy 2017;141:1928−39. https://doi.org/10.1016/j.energy.2017.10.142.

[10] Jouhara H, Khordehgah N, Almahmoud S, Delpech B, Chauhan A, Tassou SA. Waste heat recovery technologies and applications. Therm Sci Eng Prog 2018;6:268−89. https://doi.org/10.1016/j.tsep.2018.04.017.

[11] Jouhara H, Szulgowska-Zgrzywa M, Sayegh MA, Milko J, Danielewicz J, Nannou TK, et al. The performance of a heat pipe based solar PV/T roof collector and its potential contribution in district heating applications. Energy 2017;136:117−25. https://doi.org/10.1016/j.energy.2016.04.070.

[12] Jouhara H, Meskimmon R. Heat pipe based thermal management systems for energy-efficient data centres. Energy 2014;77:265−70. https://doi.org/10.1016/j.energy.2014.08.085.

[13] Shabgard H, Allen MJ, Sharifi N, Benn SP, Faghri A, Bergman TL. Heat pipe heat exchangers and heat sinks: opportunities, challenges, applications, analysis, and state of the art. Int J Heat Mass Tran 2015;89:138−58. https://doi.org/10.1016/j.ijheatmasstransfer.2015.05.020.

[14] Amini A, Miller J, Jouhara H. An investigation into the use of the heat pipe technology in thermal energy storage heat exchangers. Energy 2017;136:163−72. https://doi.org/10.1016/j.energy.2016.02.089.

[15] Jouhara H, Nannou TK, Anguilano L, Ghazal H, Spencer N. Heat pipe based municipal waste treatment unit for home energy recovery. Energy; 2017. https://doi.org/10.1016/j.energy.2017.02.044.

[16] Jouhara H, Chauhan A, Nannou T, Almahmoud S, Delpech B, Wrobel LC. Heat pipe based systems - advances and applications. Energy 2017;128:729−54. https://doi.org/10.1016/j.energy.2017.04.028.

[17] Jouhara H. Economic assessment of the benefits of wraparound heat pipes in ventilation processes for hot and humid climates. Int J Low Carbon Technol 2009;4:52−60. https://doi.org/10.1093/ijlct/ctp006.

[18] Jouhara H, Robinson AJ. An experimental study of small-diameter wickless heat pipes operating in the temperature range 200c to 450c. Heat Tran Eng 2009;30:1041−8. https://doi.org/10.1080/01457630902921113.

[19] Cengel YA. Heat transfer: a practical approach. New York McGraw-Hill; 2003. p. 785−841. https://doi.org/10.1017/CBO9781107415324.004.

[20] Bergman TL, Incropera FP, DeWitt DP, Lavine AS. Fundamentals of heat and mass transfer. John Wiley & Sons; 2011.

[21] Ramos J, Chong A, Jouhara H. Experimental and numerical investigation of a cross flow air-to-water heat pipe-based heat exchanger used in waste heat recovery. Int J Heat Mass Tran 2016;102:1267−81. https://doi.org/10.1016/j.ijheatmasstransfer.2016.06.100.

[22] Mroue H, Ramos JB, Wrobel LC, Jouhara H. Experimental and numerical investigation of an air-to-water heat pipe-based heat exchanger. Appl Therm Eng 2015;78:339−50. https://doi.org/10.1016/j.applthermaleng.2015.01.005.

[23] Kim M-S, Lee K-S, Song S. Effects of pass arrangement and optimization of design parameters on the thermal performance of a multi-pass heat exchanger. Int J Heat Fluid Flow 2008;29:352−63. https://doi.org/10.1016/J.IJHEATFLUIDFLOW.2007.05.010.

[24] Rao BP, Das SK. Effect of flow distribution to the channels on the thermal performance of the multipass plate heat exchangers. Heat Tran Eng 2004;25:48−59. https://doi.org/10.1080/01457630490520284.

[25] Thulukkanam K. Heat exchanger design handbook. Boca Raton: CRC press; 2013.

[26] Danielewicz J, Sayegh MA, Śniechowska B, Szulgowska-Zgrzywa M, Jouhara H. Experimental and analytical performance investigation of air to air two phase closed thermosyphon based heat exchangers. Energy 2014;77:82−7. https://doi.org/10.1016/j.energy.2014.04.107.

[27] Jouhara H, Merchant H. Experimental investigation of a thermosyphon based heat exchanger used in energy efficient air handling units. Energy 2012;39:82−9. https://doi.org/10.1016/j.energy.2011.08.054.

[28] Brough D, Ramos J, Delpech B, Jouhara H. Development and validation of a TRNSYS type to simulate heat pipe heat exchangers in transient applications of waste heat recovery. Int J Thermofluids 2020. https://doi.org/10.1016/j.ijft.2020.100056. Accepted.

[29] Noie SH. Investigation of thermal performance of an air-to-air thermosyphon heat exchanger using ε-NTU method. Appl Therm Eng 2006;26:559−67. https://doi.org/10.1016/J.APPLTHERMALENG.2005.07.012.

[30] Mroue H, Ramos JB, Jouhara H. Performance evaluation of a multi-pass air-to-water thermosyphon-based heat exchanger. Energy 2017. https://doi.org/10.1016/j.energy.2017.04.111.

[31] Hua N, Xi H, Xu RJ, Chen Y, Wang HS. Numerical simulation of multi-pass parallel flow condensers with liquid-vapor separation. Int J Heat Mass Tran 2019;142:118469. https://doi.org/10.1016/J.IJHEATMASSTRANSFER.2019.118469.

[32] Rohsenow Editor WM, Hartnett Editor JR, Cho Editor YI, San NY, Washington F, Auckland DC, et al. Handbook of heat transfer. 1998.

[33] Nusselt W. The condensation of steam on cooled surfaces. Z Ver Dtsch Ing 1916;60:541−6.

[34] Guichet V, Jouhara H. Condensation, evaporation and boiling of falling films in wickless heat pipes (two-phase closed thermosyphons): a critical review of correlations. Int J Thermofluids 2019:100001. https://doi.org/10.1016/j.ijft.2019.100001.

[35] Rohsenow WM. A method of correlating heat-transfer data for surface boiling of liquids. 1952.

[36] Guichet V, Almahmoud S, Jouhara H. Nucleate pool boiling heat transfer in wickless heat pipes (two-phase closed thermosyphons): a critical review of correlations. Therm Sci Eng Prog 2019;13. https://doi.org/10.1016/j.tsep.2019.100384.

[37] Kakac S, Shah RK, Aung W. Handbook of single-phase convective heat transfer. United States: John Wiley and Sons Inc; 1987.

[38] Žukauskas A. Heat transfer from tubes in crossflow. Adv Heat Tran 1972;8:93−160. https://doi.org/10.1016/S0065-2717(08)70038-8.

[39] Azad E, Geoola F. A design procedure for gravity-assisted heat pipe heat exchanger. J Heat Recovery Syst 1984;4:101−11. https://doi.org/10.1016/0198-7593(84)90014-6.

[40] Magazoni FC, Cabezas-Gómez L, Alvariño PF, Sáiz-Jabardo JM. Closed form relationships of temperature effectiveness of cross-flow heat exchangers. Therm Sci Eng Prog 2019;9:110−20. https://doi.org/10.1016/J.TSEP.2018.11.005.

[41] Eurostat. Gas prices by type of user- EU (27 countries). 2020. https://ec.europa.eu/eurostat/tgm/graph.do?tab=graph&plugin=1&pcode=ten00118&language=en&toolbox=data. [Accessed 10 September 2020].

[42] Taylor J. Introduction to error analysis, the study of uncertainties in physical measurements. 1997.